
What to Ignore, What to React: Visually Robust RL Fine-Tuning of VLA Models

Yuanfang Peng^{1,2} Jingjing Fu² Chuheng Zhang² Li Zhao² Jiang Bian²
Mingyu Liu³ Ling Zhang^{2*} Jun Zhang^{1*} Rui Wang^{2*}

¹Hong Kong University of Science and Technology

²Microsoft Research Asia

³Zhejiang University

ypengbx@connect.ust.hk, eejzhang@ust.hk

{ds.dashu, jiang.bian.prc, wrui0920}@gmail.com

{chuhengzhang, lizo, zhangling}@microsoft.com

Abstract

Reinforcement learning (RL) fine-tuning has shown promise for Vision-Language-Action (VLA) models in robotic manipulation, but deployment-time visual shifts pose practical challenges. A key difficulty is that standard task rewards supervise task success, but offer limited guidance on whether a visual change is task-irrelevant or changes the behavior required for manipulation. We propose PAIR-VLA (Paired Action Invariance & Sensitivity for Visually Robust VLA), an RL fine-tuning framework to address this difficulty by adding two auxiliary objectives over paired visual variants during PPO optimization: an invariance term that reduces the discrepancy between action distributions for a task-preserving pair (e.g., different distractors), and a sensitivity objective that encourages separable action distributions for a task-altering pair (e.g., target object in a different pose). Together, these objectives turn visual variants from mere observation diversity into behavior-level guidance on policy responses during RL fine-tuning. Because the auxiliary objectives are used only during RL fine-tuning, deployment will use the same policy architecture, thus incurring no additional inference-time cost. We evaluate on ManiSkill3 across two representative VLA architectures, OpenVLA and $\pi_{0.5}$, under diverse out-of-distribution visual shifts including unseen distractors, texture changes, target object pose variation, viewpoint shifts, and lighting changes. Our method consistently improves over standard PPO, achieving average absolute improvements of 16.62% on $\pi_{0.5}$ and 9.10% on OpenVLA. Notably, ablations further show generalization across visual shifts: invariance guidance learned from distractor and texture variants transfers to target-pose and lighting shifts, while adding sensitivity guidance on target-pose variants further improves robustness to nuisance shifts, highlighting the broader transferability of behavior-level RL guidance.

1 Introduction

Vision-Language-Action (VLA) models, pretrained on internet-scale vision-language data and diverse robot demonstrations [1, 2], have emerged as a promising paradigm for general-purpose robotic manipulation [3, 4, 5]. However, pretraining does not guarantee robustness under visual shifts at deployment. Policies may remain sensitive to nuisance changes such as lighting, scene texture, or the presence of distractor objects [6, 7], even when these changes do not alter the underlying manipulation objective. These variations are challenging not only because they change the visual input, but also

*Corresponding authors.

because they have different consequences for action: some should leave the intended manipulation unchanged, while others require the policy to adjust its behavior. Such action-dependent visual shifts remain a challenge when adapting VLA policies to downstream manipulation tasks.

Reinforcement learning (RL) fine-tuning has recently been explored as a post-training approach for improving VLA policies on downstream manipulation tasks [8, 9, 10, 11, 12]. Unlike supervised fine-tuning (SFT) on fixed demonstrations, RL optimizes expected task rewards through interaction, allowing the policy to adapt beyond the demonstration distribution. However, visual robustness remains an important challenge during RL fine-tuning, as policies can still exhibit limited generalization under deployment-time visual shifts [10, 13]. This raises the question of how visual variation should be incorporated into the RL fine-tuning process.

Existing approaches often improve generalization by increasing the diversity of training observations. In visual RL, image-level augmentations such as random cropping or color perturbation have been widely used to improve perceptual robustness [14, 15, 16]. In robotics and sim-to-real learning, domain randomization is commonly applied over textures, lighting, camera poses, object placements, and distractor configurations [17, 18, 19]. These techniques are effective in many settings, but they primarily expose the policy to more varied observations. However, in RL-based VLA fine-tuning, observation diversity alone does not inform the policy how its actions should respond to different types of scene changes, i.e., which changes should be ignored, and which changes should alter the required manipulation. This behavioral distinction is central to visual generalization in RL fine-tuning. The same policy should be invariant to changes that do not alter the required manipulation, while being sensitive to changes that do. We therefore study how to guide VLA policies during RL so that scene-level variation is aligned with action-level responses.

Our method, PAIR-VLA (Paired Action Invariance & Sensitivity for Visually Robust VLA), encourages two complementary behaviors: maintaining action consistency under task-irrelevant variations, and adapting actions when scene changes alter the required manipulation. Specifically, during RL training, we construct two perturbed views of each observation: a task-preserving view, where nuisance visual factors are altered while preserving the underlying task state, and a task-altering view, where the target object is perturbed. We then add two auxiliary objectives to PPO [20]: an invariance objective that aligns the action distributions induced by the original and task-preserving views, and a sensitivity objective that separates those induced by the original and task-altering views. This turns visual variants from mere observation diversity into explicit behavior-level supervision, specifying which scene changes the policy should ignore and which should induce a different action response.

We evaluate our approach on ManiSkill3 [21] with two representative VLA architectures: the autoregressive OpenVLA [22] and the flow-based $\pi_{0.5}$ [23]. Across a broad suite of out-of-distribution visual shifts, including unseen distractors, texture changes, target object pose variation, viewpoint shifts, and altered lighting conditions, our method consistently outperforms standard PPO fine-tuning, improving average success rates by 16.62% on $\pi_{0.5}$ and 9.1% on OpenVLA. Moreover, the policy generalizes to unseen lighting changes even though lighting was not used to construct the auxiliary objectives. Ablations show that invariance guidance transfers to other unseen shifts, such as target pose, while adding sensitivity guidance further improves robustness to nuisance changes, highlighting the broader generalization enabled by behavior-level RL guidance.

In summary, our contributions are as follows:

- We formulate visual generalization in VLA RL fine-tuning as behavior-level guidance over policy responses to visual shifts, which can reduce the reliance on extensive observation diversity during training and improve transfer to out-of-distribution scenes.
- We propose PAIR-VLA, a PPO-compatible invariance–sensitivity framework that implements behavior-level guidance over action distributions using paired visual variants. The invariance objective stabilizes actions under task-preserving visual changes, while the sensitivity objective encourages adaptive actions when task-relevant scene state changes. These auxiliary objectives are applied only during RL fine-tuning, leaving the deployed policy and inference cost unchanged.
- We validate our method on ManiSkill3 with OpenVLA and $\pi_{0.5}$, showing consistent OOD improvements over PPO across diverse visual shifts. Ablations demonstrate that invariance and sensitivity guidance enable behavior-level RL generalization to unseen shifts.

2 Related Work

Online RL Fine-Tuning for VLA Models. Recent work has increasingly explored online RL as a post-training stage for VLA models, enabling policies pretrained or fine-tuned by supervised learning to further improve through environment interaction and task-completion rewards. FLaRe [24] introduces stabilization techniques for PPO fine-tuning of multi-task BC-pretrained policies; SimpleVLA [8] applies GRPO to OpenVLA-OFT [25]; and RLinf [9, 12] provides a unified, efficient framework for scalable RL training of VLA models. Meanwhile, RL4VLA [10] evaluates OpenVLA generalization under PPO, GRPO, and DPO, finding PPO more effective for VLAs than LLM-derived methods such as DPO and GRPO, which motivates our use of PPO as the base algorithm. More recently, π_{RL} [11] studies online RL for flow-based VLA models such as π_0 and $\pi_{0.5}$. However, RL4VLA also reports that RL performs comparably to SFT on vision tasks, hypothesizing that neither training paradigm induces visual robustness beyond the visual randomness present during training. Rather than relying on data diversity alone during training, we augment PPO with action-distribution objectives that directly shape policy responses to different visual changes, improving robustness beyond the training distribution.

Visual Robustness in Robot Manipulation. Multiple lines of research have studied how to improve visual robustness in robot learning and reduce the influence of nuisance visual variation. One direct strategy is to modify observations at inference time. For example, prior work learns masks to suppress visual distractors [26], or uses external segmentation and image editing modules, such as inpainting, to remove irrelevant visual content before feeding observations to the policy [27, 28, 29]. While such methods can reduce the effect of distractors at deployment, they require extra modules to identify or remove irrelevant visual content at inference time, and do not directly train the policy itself to decide which visual changes should affect its behavior.

A more common training-time strategy is to expose the policy to more diverse visual observations. In visual RL, image-level augmentations such as random cropping, color perturbation, and random shifts are widely used when learning policies from pixels [14, 15, 16]. In sim-to-real robot learning, domain randomization varies simulation parameters such as textures, lighting, camera poses, object placements, and distractor configurations to reduce the visual gap between simulation and deployment [17, 18, 19]. Generative image editing, including inpainting and image synthesis, has also been used to create more realistic or diverse training observations [30, 31]. These methods improve robustness through broader observation diversity, but do not specify how the policy’s actions should respond to different types of scene changes.

Another line of work regularizes visual representations across perturbed views. These methods encourage invariance across perturbed observations through representation learning objectives, including contrastive learning, bisimulation-based state abstraction, and consistency regularization in feature or value space [32, 33, 34, 35, 36, 37]. Related approaches use information bottleneck to learn only task-relevant visual representations [38, 39]. These approaches provide useful representation-level regularization, but invariance in latent space does not necessarily guarantee the desired behavior at the action-distribution level.

Recent work has begun to incorporate robustness-aware objectives into RL post-training. Closest to our setting, RobustVLA [13] improves the resilience of VLA policies to observation noise and action perturbations during online RL training using Jacobian and smoothness regularization. Our setting differs in that we target broader scene-level visual shifts in robot manipulation, such as changes in distractor objects and target location. Such shifts are not merely local corruptions, but can change whether the policy should preserve or adapt its manipulation behavior. BiPS [40] introduces consistency and separation objectives during RL training of VLMs for visual question answering. While we draw inspiration from this principle, VLA policy learning differs from VLM reasoning in the output space, the role of visual changes, and the policy architectures used to generate actions. We therefore ground the consistency–separation signal in manipulation consequences, using paired visual variants to keep policy behavior stable under task-preserving changes and adapt under task-altering changes. This allows visual variations to serve as behavior-level guidance during RL fine-tuning, while leaving the deployed VLA policy architecture unchanged.

3 Preliminaries

Language-Conditioned Manipulation. We model language-conditioned robotic manipulation as a partially observable Markov decision process (POMDP), defined as a tuple $\mathcal{M} = (\mathcal{S}, \mathcal{A}, \mathcal{P}, R, \mathcal{O}, \gamma)$, augmented with a language instruction space \mathcal{L} . At the beginning of each episode, the robot receives a natural language instruction $l \in \mathcal{L}$, which remains fixed throughout the episode. At each time step t , the robot observes $o_t \in \mathcal{O}$ as a partial view of the underlying state $s_t \in \mathcal{S}$, and outputs an action $a_t \sim \pi_\theta(\cdot | o_t, l)$, where π_θ denotes the policy. The environment transitions follow $s_{t+1} \sim \mathcal{P}(\cdot | s_t, a_t)$.

Vision-Language-Action Models. We instantiate the policy $\pi_\theta(\cdot | o, l)$ using VLA models, which map visual observations and language instructions to robot actions. We consider two representative architectures of VLA models: autoregressive models (e.g., OpenVLA [22]), and flow-matching models (e.g., $\pi_{0.5}$ [23]). Our method applies to both architectures.

RL fine-tuning and PPO. We use Proximal Policy Optimization (PPO) [20] as our RL fine-tuning baseline, due to its empirical stability and effectiveness in continuous control settings [10, 11]. Given an old policy $\pi_{\theta_{\text{old}}}$, PPO optimizes the clipped surrogate objective

$$\mathcal{J}_{\text{PPO}}(\theta) = \mathbb{E}_{\tau \sim \pi_{\theta_{\text{old}}}} \left[\frac{1}{T} \sum_{t=1}^T \min \left(w_t(\theta) \hat{A}_t, \text{clip} \left(w_t(\theta), 1 - \epsilon, 1 + \epsilon \right) \hat{A}_t \right) \right], \quad (1)$$

where $w_t(\theta) = \frac{\pi_\theta(a_t|o_t,l)}{\pi_{\theta_{\text{old}}}(a_t|o_t,l)}$ is the likelihood ratio between the updated and old policies, ϵ is the clipping parameter, and \hat{A}_t denotes the advantage estimate computed using Generalized Advantage Estimation (GAE) [41].

PPO can be applied directly to autoregressive VLAs via their explicit action log-likelihoods. Flow-matching VLAs, however, generate actions through iterative ODE denoising and lack tractable action log probabilities, making the standard PPO likelihood-ratio objective difficult to apply directly. We follow π_{RL} [11], which converts the ODE denoising process into an SDE and formulates a two-layer MDP. This yields tractable log-likelihoods and enables PPO updates.

4 Visual Robustness via Invariance and Sensitivity Objectives

4.1 Problem Formulation

Our goal is to learn a policy that is robust to task-irrelevant visual variations while remaining sensitive to task-relevant ones. Consider a policy $a \sim \pi_\theta(\cdot | o, l)$ conditioned on an observation o and a language instruction l . We define a visually robust policy as one satisfying two properties: (1) *task-preserving invariance*: the action distribution is approximately preserved under task-irrelevant visual perturbations, including the presence of distractor objects, changes in viewpoint, and changes in background appearance such as table textures; (2) *task-altering sensitivity*: the action distribution changes meaningfully under perturbations to the task-relevant objects.

To operationalize these properties during RL fine-tuning, we introduce controlled perturbations of the input observation by constructing two types of perturbed views. The first is a *task-preserving view*, which removes distractor objects and varies background appearance factors such as textures and colors while preserving the underlying task state and required manipulation. The second is a *task-altering view*, which modifies task-relevant properties of the target object (e.g., object pose) while preserving its semantic identity.

These views instantiate the task-irrelevant and task-relevant visual changes used by our auxiliary objectives.

4.2 Invariance and Sensitivity Objectives

Using the task-preserving and task-altering views, we add two complementary auxiliary objectives to PPO training. Both are formulated as KL divergences between the action distributions induced by the original and perturbed observations. The invariance objective aligns the policy distribution under the original and task-preserving views, encouraging consistency under visual changes that preserve the

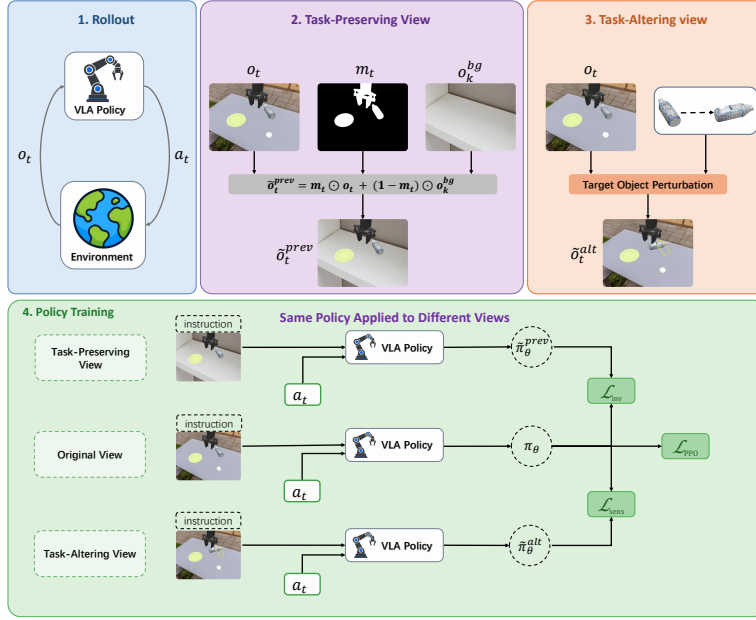


Figure 1: Overview of the visually robust RL fine-tuning framework. At each environment step, the VLA policy receives an observation o_t from the environment and samples an action a_t . Based on o_t , the task-preserving view is constructed by removing distractors and changing background appearance, while the task-altering view is constructed by perturbing the pose of the target object. During policy training, the original view and paired variants are separately passed through the same VLA policy π_θ to compute their action distributions. The invariance and sensitivity objectives are computed over these action distributions, and optimized as auxiliary objectives during PPO training.

required manipulation. The sensitivity objective separates the policy distribution under the original and task-altering views, encouraging the policy to respond when the required manipulation changes.

Invariance objective. To enforce task-preserving invariance, we encourage the policy to produce consistent action distributions under visual changes that do not alter the required manipulation. Let $\tilde{o}_t^{\text{prev}}$ denote the task-preserving view of o_t . We then minimize the KL divergence between the action distributions induced by the original and task-preserving views:

$$\mathcal{L}_{\text{inv}}(\theta) = \mathbb{E}_{(o_t, l)} \left[D_{\text{KL}}(\pi_\theta(\cdot | o_t, l) \parallel \text{sg}[\pi_\theta(\cdot | \tilde{o}_t^{\text{prev}}, l)]) \right], \quad (2)$$

where $\text{sg}[\cdot]$ denotes the stop-gradient operator. It treats the task-preserving-view distribution as a fixed target to stabilize training.

Sensitivity objective.

The invariance objective specifies which visual changes should leave the policy distribution unchanged, but provides no signal for which changes should alter it. In manipulation, task-relevant changes such as target object pose can require different grasps, motions, or placements. We therefore introduce a sensitivity objective that provides the complementary signal, explicitly encouraging the policy distribution to change under task-altering perturbations.

Let \tilde{o}_t^{alt} denote the task-altering view of o_t . We then maximize the KL divergence between the action distributions induced by the original and task-altering views:

$$\mathcal{L}_{\text{sens}}(\theta) = -\mathbb{E}_{(o_t, l)} \left[\min(c, D_{\text{KL}}(\pi_\theta(\cdot | o_t, l) \parallel \text{sg}[\pi_\theta(\cdot | \tilde{o}_t^{\text{alt}}, l)]) \right], \quad (3)$$

where c is a clipping threshold that prevents unbounded divergence growth from destabilizing PPO training.

Augmented PPO objective. Combining the invariance and sensitivity objectives with the standard PPO objective, we obtain the overall training objective:

$$\mathcal{L}(\theta) = \mathcal{L}_{\text{PPO}}(\theta) + \alpha \mathcal{L}_{\text{inv}}(\theta) + \beta \mathcal{L}_{\text{sens}}(\theta), \quad (4)$$

where $\alpha, \beta > 0$ are coefficients controlling the relative strength of each auxiliary objective. The two terms are complementary: \mathcal{L}_{inv} discourages the policy from responding to task-irrelevant visual changes, while $\mathcal{L}_{\text{sens}}$ encourages responsiveness to changes in task-relevant object state. Together, they provide explicit action-level guidance on which visual changes should preserve the policy’s distribution and which should alter it. Figure 1 summarizes the overall fine-tuning framework.

4.3 Augmented View Construction

We now describe how we implement the two perturbed views used by the invariance and sensitivity objectives.

Task-preserving view. The task-preserving view alters task-irrelevant visual factors while preserving the underlying task state and required manipulation. In our main construction, we instantiate this view by removing distractors and changing background appearance through foreground-background compositing. Task-relevant foreground content from the current observation is composited with background snapshots from different scene configurations. Segmentation masks for foreground extraction are obtained directly from the simulator via object identifiers; in real-world settings, they can be approximated by an off-the-shelf segmentation model such as SAM 3 [42].

Prior to training, we pre-render a set of K background snapshots $\{o_k^{\text{bg}}\}_{k=1}^K$ by rendering each scene configuration with all objects set to invisible. During training, for each observation o_t , we define a binary segmentation mask m_t that takes value 1 for pixels belonging to the robot, target object, or receptacle, and 0 otherwise. We then sample a background snapshot o_k uniformly from the pre-rendered set, and construct the task-preserving view as

$$\tilde{o}_t^{\text{prev}} = m_t \odot o_t + (1 - m_t) \odot o_k^{\text{bg}}. \quad (5)$$

This operation removes distractors and replaces background appearance while preserving task-relevant content.

To evaluate whether the proposed invariance objective can improve generalization to unseen viewpoints, we also construct an alternative task-preserving view for viewpoint variation in Section 5.5.

Task-altering view. The task-altering view modifies task-relevant visual content while preserving the semantic identity of the target object. We construct this view by perturbing the pose of the target object. Specifically, at each training step, we sample a translation perturbation from a Gaussian distribution and a rotation perturbation from a categorical distribution, apply them to the target object, and re-render the scene to obtain \tilde{o}_t^{alt} . This produces target object pose variations that can change the required grasp, motion, or placement. In simulation, we implement this by directly setting the object pose through the simulator API.

5 Experiments

We evaluate whether our method improves the visual robustness of RL-fine-tuned VLA models across visual shifts. The experiments are designed to answer four questions: (1) whether the proposed auxiliary objectives improve OOD generalization over standard PPO, (2) whether they improve RL fine-tuning efficiency, (3) how each objective contributes to performance, and (4) whether the proposed method generalizes to other task-preserving visual changes such as viewpoint shifts.

5.1 Experimental Setup

Models and Training. For the autoregressive VLA, we use OpenVLA [22]; for the flow-matching VLA, we use $\pi_{0.5}$ [23]. For each backbone, we first obtain an SFT checkpoint and use it to initialize both the PPO baseline and our method. We then fine-tune both models under the same PPO settings, where our method augments PPO with the proposed auxiliary objectives. Details of the SFT procedure, PPO settings, and auxiliary-objective hyperparameters are provided in Appendix A.

Benchmark. We conduct experiments in the Maniskill3 [21] simulator and focus on a representative *pick-and-place* task with visual distractors, where the agent must place a target object onto a receptacle (a plate in our setup), despite the presence of distractors.

To systematically evaluate visual robustness, we design a set of out-of-distribution (OOD) scenarios that vary visual factors beyond those seen in training. During training, target objects, distractors, and

Table 1: OOD generalization of our method compared to PPO across four OOD scenarios on OpenVLA and $\pi_{0.5}$. Values are success rates (%). The Clutter column reports the average over test settings with 2, 4, 6, and 8 distractors. Δ Avg. is computed relative to the PPO baseline.

Model	Method	OOD settings					
		Table Texture	Lighting	Target Pose	Clutter	Avg.	Δ Avg.
OpenVLA	PPO	86.98	72.14	83.59	68.88	77.90	–
	Ours	94.53	80.47	90.63	82.36	87.00	+9.10
$\pi_{0.5}$	PPO	63.54	28.54	56.46	36.46	46.25	–
	Ours	80.21	51.67	69.38	50.21	62.87	+16.62

table textures are sampled from predefined training sets. To prevent overfitting to specific spatial configurations, at the beginning of each episode, the initial positions of the target object, distractors and receptacle are randomly sampled from a 6×6 grid of discrete positions on the table surface.

At test time, we then assess generalization under OOD scenarios where the following visual factors differ from those seen during training: (1) *unseen table texture*, where table textures are sampled from a held-out set; (2) *unseen lighting*, where scene lighting is varied using unseen configurations; (3) *unseen poses*, where the target object pose is sampled from translation and rotation distributions that differ from those used during training; and (4) *unseen clutter*, where the number of distractors is increased, with half of the distractors sampled from a held-out object set. The corresponding train/test splits are provided in Appendix B.

Metrics. We evaluate performance using task success rate, defined as the fraction of evaluation episodes in which the agent successfully completes the task. For each run, success rate is computed over 128 evaluation episodes, and we report the mean across three independent runs for each task.

5.2 Main Results

OOD generalization. Table 1 reports success rates on the four OOD visual generalization settings defined above: unseen table texture, unseen lighting, unseen target pose, and unseen clutter. The Distractor column averages over test settings with 2, 4, 6, and 8 distractors, which we analyze in more detail in Section 5.4. Across both OpenVLA and $\pi_{0.5}$, our method consistently improves over PPO in every OOD setting. On OpenVLA, our method improves the average OOD success rate from 77.90% to 87.00%, yielding a gain of 9.10 points. On $\pi_{0.5}$, the improvement is larger, increasing the average success rate from 46.25% to 62.87%, for a gain of 16.62 points. These results show that adding our auxiliary objectives to PPO improves visual generalization across both autoregressive and flow-based VLA backbones.

RL Fine-Tuning Efficiency. To further assess whether our method improves the fine-tuning efficiency of PPO, we periodically evaluate OpenVLA checkpoints obtained at different training steps on both an in-distribution (ID) scenario (Fig. 2a) and an OOD scenario (Fig. 2b). In the ID scenario, the scene contains one distractor sampled from the same object set used during training. In the OOD scenario, the scene contains four distractors, half sampled from the training object set and half from a held-out object set.

In the ID scenario, our method reaches a success rate of 90% within 80 training steps, whereas PPO requires roughly 240 steps to reach the same level, yielding an approximate $3\times$ improvement in fine-tuning efficiency. The advantage also holds in the OOD scenario. These results indicate that our auxiliary objectives improve not only final OOD robustness but also the efficiency of PPO fine-tuning.

5.3 Ablation Study

We ablate the two auxiliary objectives in our method, the invariance objective \mathcal{L}_{inv} and the sensitivity objective \mathcal{L}_{sens} , using the $\pi_{0.5}$ backbone on Maniskill3. Table 2 reports OOD success rates under the same four OOD settings as in Table 1. Adding \mathcal{L}_{inv} alone yields a large average gain of +12.61 points over PPO, with particularly strong improvements under unseen lighting (+16.04) and unseen clutter (+13.54). \mathcal{L}_{sens} alone gives a smaller but consistent gain of +1.73 points, but combining it

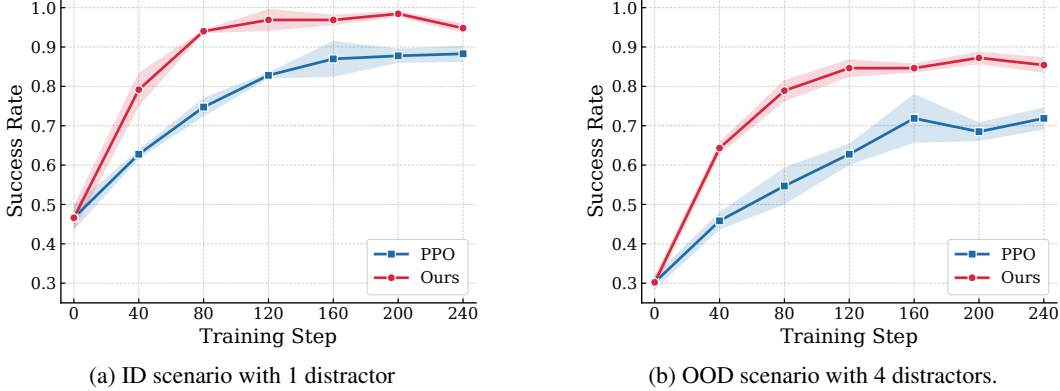


Figure 2: **RL fine-tuning efficiency on Maniskill3 with OpenVLA.** Success rate versus training step for our method and PPO on (a) an ID scenario and (b) an OOD clutter scenario. Solid lines show the mean over three seeds; shaded regions show the standard deviation. Our method converges substantially faster and reaches a higher plateau in both settings.

Table 2: Ablation of the two auxiliary objectives using the $\pi_{0.5}$ backbone. Values are success rates (%). The Clutter column reports the average over test settings with 2, 4, 6, and 8 distractors. Δ Avg. is computed relative to the PPO baseline.

Method	OOD settings					
	Table Texture	Lighting	Target Pose	Clutter	Avg.	Δ Avg.
PPO	63.54	28.54	56.46	36.46	46.25	–
PPO w/ \mathcal{L}_{inv}	72.92	44.58	67.92	50.00	58.86	+12.61
PPO w/ \mathcal{L}_{sens}	63.96	33.54	53.33	41.10	47.98	+1.73
Ours	80.21	51.67	69.38	50.21	62.87	+16.62

with \mathcal{L}_{inv} achieves the best results across all four OOD settings, improving over PPO by +16.62 points on average. This suggests that the invariance objective provides the main robustness signal, while the sensitivity objective further improves robustness when used jointly.

5.4 Analysis

OOD generalization under increasing clutter levels. We further analyze OOD generalization under varying clutter levels by evaluating OpenVLA and $\pi_{0.5}$ with 2 to 8 distractors; in each setting, half of the distractors are sampled from a held-out object set (Figures 3a and 3b). As expected, success rates decrease for both PPO and our method as the number of unseen distractors increases. However, our method consistently maintains higher success rates across all tested clutter levels, showing a more robust degradation profile. In the most challenging setting with 8 distractors, our method achieves 72% on OpenVLA and 33% on $\pi_{0.5}$, compared to 56% and 21% for PPO, respectively.

Effect of the Invariance Coefficient α . Since the invariance objective provides the dominant robustness gain in the ablation study, we further examine how its weight affects OOD generalization. We sweep $\alpha \in \{0, 1, 2, 4\}$ using the $\pi_{0.5}$ backbone while disabling the sensitivity objective by setting $\beta = 0$, so that $\alpha = 0$ recovers the PPO baseline. Figure 4 reports success rates under the four OOD settings: unseen table texture, unseen lighting, unseen target pose, and unseen clutter. Across all settings, enabling the invariance objective improves over PPO. The best performance is obtained at $\alpha = 1$, which yields gains of more than 10 points in each OOD setting and more than 15 points under unseen lighting, although lighting is not directly varied in the task-preserving view construction used for the invariance objective. Performance remains strong at $\alpha = 4$, indicating that the robustness gains are stable across different invariance weights.

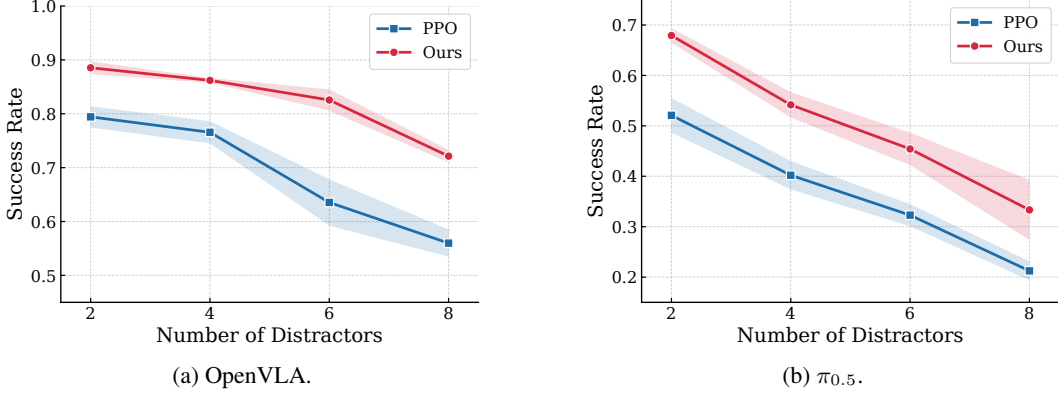


Figure 3: **OOD generalization under increasing clutter levels.** Success rate with 2–8 distractors for (a) OpenVLA and (b) $\pi_{0.5}$; half of the distractors in each setting are sampled from a held-out object set.

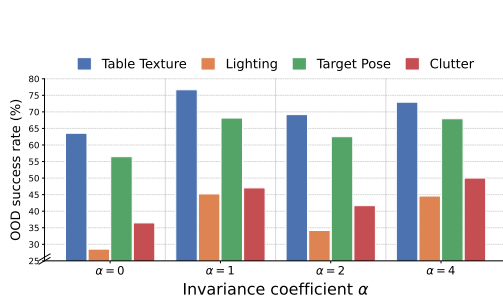


Figure 4: **Effect of the invariance coefficient α .** OOD success rates (%) on ManiSkill3 with the $\pi_{0.5}$ backbone for $\alpha \in \{0, 1, 2, 4\}$, with the sensitivity objective disabled ($\beta = 0$). Here, $\alpha = 0$ recovers the PPO baseline. Nonzero values of α consistently improve OOD performance, with $\alpha = 1$ achieving the best overall results and gains remaining stable across the tested invariance weights.

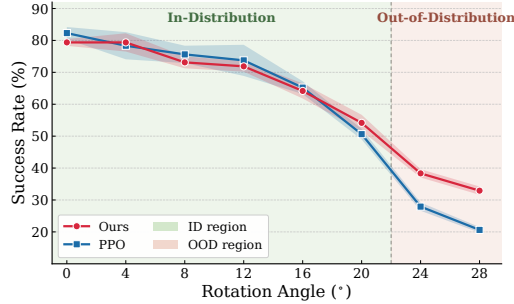


Figure 5: **OOD extrapolation to unseen camera poses with $\pi_{0.5}$.** Success rate versus camera rotation angle. Green and salmon shading mark the training range $[0^\circ, 20^\circ]$ and unseen angles $\{24^\circ, 28^\circ\}$, respectively. Lines denote the mean over three seeds, with bands showing one standard deviation. Our method matches PPO within the training viewpoint range while significantly outperforming it under unseen camera poses.

5.5 Generalization to Unseen Camera Viewpoints

We further evaluate generalization to unseen camera viewpoints using an alternative task-preserving view for the invariance objective, where the same scene state is re-rendered from a different camera pose while preserving object poses, robot state, and the task goal. The task-altering view used for the sensitivity objective remains unchanged. During RL fine-tuning, the policy sees camera rotations within $[0^\circ, 20^\circ]$ at 4° increments. At test time, we evaluate rotations from 0° to 28° at the same 4° increments, with $\{24^\circ, 28^\circ\}$ forming the OOD range.

Figure 5 reports success rates across camera viewpoints. In the ID range, our method achieves 70.36% success, comparable to 70.97% for PPO. In the OOD range, our method substantially outperforms PPO, achieving 38.34% versus 27.92% at 24° , and 32.92% versus 20.63% at 28° . This shows that, when instantiated with viewpoint-based task-preserving views, our method improves extrapolation to OOD camera poses while preserving in-distribution performance.

6 Discussion & Conclusion

We proposed PAIR-VLA, a visually robust RL fine-tuning framework for VLA models. The framework augments PPO with two auxiliary objectives that encourage invariance to task-irrelevant visual

changes and sensitivity to task-relevant ones. On ManiSkill3, our method consistently improves OOD success rates over PPO on both OpenVLA and $\pi_{0.5}$ across diverse visual shifts, including unseen table textures, target-pose shifts, and increasing visual clutter. It improves generalization to unseen lighting conditions, even though lighting changes are not used to construct the paired views for our auxiliary objectives. An additional camera-pose experiment further shows improved generalization to unseen camera viewpoints. The method also improves RL fine-tuning efficiency, achieving higher in-distribution and OOD success rates with fewer PPO updates. A limitation of our current study is that evaluation is conducted in simulation, and task-preserving view construction relies on ground-truth object masks from the simulator. Future work could study whether robustness learned in simulation transfers to real-world deployment, and examine how segmentation masks estimated by off-the-shelf models affect paired-view construction and the resulting robustness gains. Importantly, both paired-view construction and the auxiliary objectives are used only during RL fine-tuning, so the deployed policy requires no additional inference-time modules.

References

- [1] Abby O’Neill, Abdul Rehman, Abhiram Maddukuri, Abhishek Gupta, Abhishek Padalkar, Abraham Lee, Acorn Pooley, Agrim Gupta, Ajay Mandlekar, Ajinkya Jain, et al. Open x-embodiment: Robotic learning datasets and rt-x models: Open x-embodiment collaboration 0. In *2024 IEEE International Conference on Robotics and Automation (ICRA)*, pages 6892–6903. IEEE, 2024.
- [2] Alexander Khazatsky, Karl Pertsch, Suraj Nair, Ashwin Balakrishna, Sudeep Dasari, Siddharth Karamcheti, Soroush Nasiriany, Mohan Kumar Srirama, Lawrence Yunliang Chen, Kirsty Ellis, et al. Droid: A large-scale in-the-wild robot manipulation dataset. *arXiv preprint arXiv:2403.12945*, 2024.
- [3] Anthony Brohan, Noah Brown, Justice Carbajal, Yevgen Chebotar, Xi Chen, Krzysztof Choro-manski, Tianli Ding, Danny Driess, Avinava Dubey, Chelsea Finn, Pete Florence, Chuyuan Fu, Montse Gonzalez Arenas, Keerthana Gopalakrishnan, Kehang Han, Karol Hausman, Alexander Herzog, Jasmine Hsu, Brian Ichter, Alex Irpan, Nikhil Joshi, Ryan Julian, Dmitry Kalashnikov, Yuheng Kuang, Isabel Leal, Lisa Lee, Tsang-Wei Edward Lee, Sergey Levine, Yao Lu, Henryk Michalewski, Igor Mordatch, Karl Pertsch, Kanishka Rao, Krista Reymann, Michael Ryoo, Grecia Salazar, Pannag Sanketi, Pierre Sermanet, Jaspier Singh, Anikait Singh, Radu Soricut, Huang Tran, Vincent Vanhoucke, Quan Vuong, Ayzaan Wahid, Stefan Welker, Paul Wohlhart, Jialin Wu, Fei Xia, Ted Xiao, Peng Xu, Sichun Xu, Tianhe Yu, and Brianna Zitkovich. Rt-2: Vision-language-action models transfer web knowledge to robotic control, 2023.
- [4] Octo Model Team, Dibya Ghosh, Homer Walke, Karl Pertsch, Kevin Black, Oier Mees, Sudeep Dasari, Joey Hejna, Tobias Kreiman, Charles Xu, Jianlan Luo, You Liang Tan, Lawrence Yunliang Chen, Pannag Sanketi, Quan Vuong, Ted Xiao, Dorsa Sadigh, Chelsea Finn, and Sergey Levine. Octo: An open-source generalist robot policy, 2024.
- [5] Kevin Black, Noah Brown, Danny Driess, Adnan Esmail, Michael Equi, Chelsea Finn, Niccolo Fusai, Lachy Groom, Karol Hausman, Brian Ichter, et al. π_0 : A vision-language-action flow model for general robot control. *arXiv preprint arXiv:2410.24164*, 2024.
- [6] Kaylee Burns, Zach Witzel, Jubayer Ibn Hamid, Tianhe Yu, Chelsea Finn, and Karol Hausman. What makes pre-trained visual representations successful for robust manipulation?, 2023.
- [7] Youguang Xing, Xu Luo, Junlin Xie, Lianli Gao, Hengtao Shen, and Jingkuan Song. Shortcut learning in generalist robot policies: The role of dataset diversity and fragmentation, 2025.
- [8] Haozhan Li, Yuxin Zuo, Jiale Yu, Yuhao Zhang, Zhaohui Yang, Kaiyan Zhang, Xuekai Zhu, Yuchen Zhang, Tianxing Chen, Ganqu Cui, Dehui Wang, Dingxiang Luo, Yuchen Fan, Youbang Sun, Jia Zeng, Jiangmiao Pang, Shanghang Zhang, Yu Wang, Yao Mu, Bowen Zhou, and Ning Ding. Simplevla-rl: Scaling vln training via reinforcement learning, 2025.
- [9] Chao Yu, Yuanqing Wang, Zhen Guo, Hao Lin, Si Xu, Hongzhi Zang, Quanlu Zhang, Yongji Wu, Chunyang Zhu, Junhao Hu, et al. Rlinf: Flexible and efficient large-scale reinforcement learning via macro-to-micro flow transformation. *arXiv preprint arXiv:2509.15965*, 2025.
- [10] Jijia Liu, Feng Gao, Bingwen Wei, Xinlei Chen, Qingmin Liao, Yi Wu, Chao Yu, and Yu Wang. What can rl bring to vln generalization? an empirical study, 2026.
- [11] Kang Chen, Zhihao Liu, Tonghe Zhang, Zhen Guo, Si Xu, Hao Lin, Hongzhi Zang, Xiang Li, Quanlu Zhang, Zhaofei Yu, Guoliang Fan, Tiejun Huang, Yu Wang, and Chao Yu. π_{RL} : Online rl fine-tuning for flow-based vision-language-action models, 2026.
- [12] Hongzhi Zang, Mingjie Wei, Si Xu, Yongji Wu, Zhen Guo, Yuanqing Wang, Hao Lin, Peihong Wang, Liangzhi Shi, Yuqing Xie, Zhexuan Xu, Zhihao Liu, Kang Chen, Wenhao Tang, Quanlu Zhang, Weinan Zhang, Chao Yu, and Yu Wang. Rlinf-vln: A unified and efficient framework for reinforcement learning of vision-language-action models, 2026.
- [13] Hongyin Zhang, Shuo Zhang, Junxi Jin, Qixin Zeng, Runze Li, and Donglin Wang. Robustvln: Robustness-aware reinforcement post-training for vision-language-action models. *arXiv preprint arXiv:2511.01331*, 2025.

- [14] Ilya Kostrikov, Denis Yarats, and Rob Fergus. Image augmentation is all you need: Regularizing deep reinforcement learning from pixels, 2021.
- [15] Michael Laskin, Kimin Lee, Adam Stooke, Lerrel Pinto, Pieter Abbeel, and Aravind Srinivas. Reinforcement learning with augmented data, 2020.
- [16] Denis Yarats, Rob Fergus, Alessandro Lazaric, and Lerrel Pinto. Mastering visual continuous control: Improved data-augmented reinforcement learning, 2021.
- [17] Josh Tobin, Rachel Fong, Alex Ray, Jonas Schneider, Wojciech Zaremba, and Pieter Abbeel. Domain randomization for transferring deep neural networks from simulation to the real world. In *2017 IEEE/RSJ international conference on intelligent robots and systems (IROS)*, pages 23–30. IEEE, 2017.
- [18] Jonathan Tremblay, Aayush Prakash, David Acuna, Mark Brophy, Varun Jampani, Cem Anil, Thang To, Eric Cameracci, Shaad Boochoon, and Stan Birchfield. Training deep networks with synthetic data: Bridging the reality gap by domain randomization. In *Proceedings of the IEEE conference on computer vision and pattern recognition workshops*, pages 969–977, 2018.
- [19] Bhairav Mehta, Manfred Diaz, Florian Golemo, Christopher J Pal, and Liam Paull. Active domain randomization. In *Conference on Robot Learning*, pages 1162–1176. PMLR, 2020.
- [20] John Schulman, Filip Wolski, Prafulla Dhariwal, Alec Radford, and Oleg Klimov. Proximal policy optimization algorithms. *arXiv preprint arXiv:1707.06347*, 2017.
- [21] Stone Tao, Fanbo Xiang, Arth Shukla, Yuzhe Qin, Xander Hinrichsen, Xiaodi Yuan, Chen Bao, Xinsong Lin, Yulin Liu, Tse-kai Chan, et al. Maniskill3: Gpu parallelized robotics simulation and rendering for generalizable embodied ai. *arXiv preprint arXiv:2410.00425*, 2024.
- [22] Moo Jin Kim, Karl Pertsch, Siddharth Karamcheti, Ted Xiao, Ashwin Balakrishna, Suraj Nair, Rafael Rafailov, Ethan Foster, Grace Lam, Pannag Sanketi, et al. Openvla: An open-source vision-language-action model. *arXiv preprint arXiv:2406.09246*, 2024.
- [23] Physical Intelligence, Kevin Black, Noah Brown, James Darpinian, Karan Dhabalia, Danny Driess, Adnan Esmail, Michael Equi, Chelsea Finn, Niccolo Fusai, et al. $\pi_{0.5}$: A vision-language-action model with open-world generalization. *arXiv preprint arXiv:2504.16054*, 2025.
- [24] Jiaheng Hu, Rose Hendrix, Ali Farhadi, Aniruddha Kembhavi, Roberto Martín-Martín, Peter Stone, Kuo-Hao Zeng, and Kiana Ehsani. Flare: Achieving masterful and adaptive robot policies with large-scale reinforcement learning fine-tuning. In *2025 IEEE International Conference on Robotics and Automation (ICRA)*, pages 3617–3624. IEEE, 2025.
- [25] Moo Jin Kim, Chelsea Finn, and Percy Liang. Fine-tuning vision-language-action models: Optimizing speed and success, 2025.
- [26] Bram Grooten, Tristan Tomilin, Gautham Vasan, Matthew E Taylor, A Rupam Mahmood, Meng Fang, Mykola Pechenizkiy, and Decebal Constantin Mocanu. Madi: Learning to mask distractions for generalization in visual deep reinforcement learning. *arXiv preprint arXiv:2312.15339*, 2023.
- [27] Sangmim Song, Sarath Kodagoda, Marc Carmichael, and Karthick Thiyagarajan. Overcoming visual clutter in vision language action models via concept-gated visual distillation. *arXiv preprint arXiv:2603.10340*, 2026.
- [28] Shihan Wu, Xu Luo, Ji Zhang, Junlin Xie, Jingkuan Song, Heng Tao Shen, and Lianli Gao. Policy contrastive decoding for robotic foundation models. *arXiv preprint arXiv:2505.13255*, 2025.
- [29] Asher J. Hancock, Allen Z. Ren, and Anirudha Majumdar. Run-time observation interventions make vision-language-action models more visually robust, 2024.
- [30] Tianhe Yu, Ted Xiao, Austin Stone, Jonathan Tompson, Anthony Brohan, Su Wang, Jaspier Singh, Clayton Tan, Jodilyn Peralta, Brian Ichter, et al. Scaling robot learning with semantically imagined experience. *arXiv preprint arXiv:2302.11550*, 2023.

- [31] Daniel Ho, Kanishka Rao, Zhuo Xu, Eric Jang, Mohi Khansari, and Yunfei Bai. Retinagan: An object-aware approach to sim-to-real transfer. In *2021 IEEE International Conference on Robotics and Automation (ICRA)*, pages 10920–10926. IEEE, 2021.
- [32] Amy Zhang, Rowan McAllister, Roberto Calandra, Yarin Gal, and Sergey Levine. Learning invariant representations for reinforcement learning without reconstruction. *arXiv preprint arXiv:2006.10742*, 2020.
- [33] Ting Chen, Simon Kornblith, Mohammad Norouzi, and Geoffrey Hinton. A simple framework for contrastive learning of visual representations. In Hal Daumé III and Aarti Singh, editors, *Proceedings of the 37th International Conference on Machine Learning*, volume 119 of *Proceedings of Machine Learning Research*, pages 1597–1607. PMLR, 13–18 Jul 2020.
- [34] Michael Laskin, Aravind Srinivas, and Pieter Abbeel. Curl: Contrastive unsupervised representations for reinforcement learning. In *International conference on machine learning*, pages 5639–5650. PMLR, 2020.
- [35] David Bertoin, Adil Zouitine, Mehdi Zouitine, and Emmanuel Rachelson. Look where you look! saliency-guided q-networks for generalization in visual reinforcement learning. *Advances in neural information processing systems*, 35:30693–30706, 2022.
- [36] Jingbo Sun, Songjun Tu, Qichao Zhang, Ke Chen, and Dongbin Zhao. Saliency-invariant consistent policy learning for generalization in visual reinforcement learning, 2025.
- [37] Jonathan Yang, Chelsea Finn, and Dorsa Sadigh. Invariance co-training for robot visual generalization. *arXiv preprint arXiv:2512.05230*, 2025.
- [38] Stephen James and Andrew J Davison. Q-attention: Enabling efficient learning for vision-based robotic manipulation. *IEEE Robotics and Automation Letters*, 7(2):1612–1619, 2022.
- [39] Vincent Pacelli and Anirudha Majumdar. Learning task-driven control policies via information bottlenecks, 2020.
- [40] Shuoshuo Zhang, Yizhen Zhang, Jingjing Fu, Lei Song, Jiang Bian, Yujiu Yang, and Rui Wang. See less, see right: Bi-directional perceptual shaping for multimodal reasoning. *arXiv preprint arXiv:2512.22120*, 2025.
- [41] John Schulman, Philipp Moritz, Sergey Levine, Michael Jordan, and Pieter Abbeel. High-dimensional continuous control using generalized advantage estimation. *arXiv preprint arXiv:1506.02438*, 2015.
- [42] Nicolas Carion, Laura Gustafson, Yuan-Ting Hu, Shoubhik Debnath, Ronghang Hu, Didac Suris, Chaitanya Ryali, Kalyan Vasudev Alwala, Haitham Khedr, Andrew Huang, et al. Sam 3: Segment anything with concepts. *arXiv preprint arXiv:2511.16719*, 2025.
- [43] Edward J Hu, Yelong Shen, Phillip Wallis, Zeyuan Allen-Zhu, Yuanzhi Li, Shean Wang, Liang Wang, Weizhu Chen, et al. Lora: Low-rank adaptation of large language models. *Iclr*, 1(2):3, 2022.

A SFT and RL Training Details

A.1 SFT Checkpoints

The VLA models are pre-trained on large-scale demonstration data. However, they still struggle to perform the downstream tasks out-of-the-box. In that case, a SFT stage is required to warm-up the VLA models. We use the checkpoints of OpenVLA and $\pi_{0.5}$ models provided by RLinf[9]. These checkpoints are finetuned from their pre-trained models with around $16k$ demonstrations collected by motion planning. Even though these demonstrations are collected in environments where no distractor is placed on the table, we observed that models finetuned on such data still show non-trivial performance on our training task with one distractor placed on the table. We therefore use these checkpoints as initializations for RL training.

A.2 RL Training Details

LoRA finetuning For the OpenVLA model, we use Low-Rank Adaptation (LoRA)[43] for RL finetuning to reduce the computation overhead. For the $\pi_{0.5}$ model, even though the recommended training recipe from π_{RL} [11] is to train the action expert only, we observed that the OOD performance of both PPO baseline and our method can be further improved. In that case, we also apply LoRA to the VLM backbone and full-finetune the action expert. For both OpenVLA and $\pi_{0.5}$, we choose LoRA rank $r = 32$ and apply LoRA modules to all linear Layers.

Training and auxiliary-objective hyperparameters. Table 3 reports the RL fine-tuning and auxiliary-objective hyperparameters used for OpenVLA and $\pi_{0.5}$. PPO hyperparameters are shared between the PPO baseline and our method for each backbone. Our method additionally uses the auxiliary-objective coefficients α and β for the invariance and sensitivity objectives, respectively, as well as the sensitivity clipping parameter c . These auxiliary hyperparameters are selected separately for OpenVLA and $\pi_{0.5}$ because the two policy parameterizations induce KL divergences on different numerical scales. We note that c is used only in the sensitivity objective and is distinct from the PPO clipping parameter.

Compute Resources For both our method and the baseline, each experiment is conducted on $8 \times H100$ GPUs. For OpenVLA, the training process requires approximately 1 day to complete. For $\pi_{0.5}$, the training process requires approximately 3 days to complete.

B Benchmark Details

We conduct experiments in the Maniskill3[21] simulator and focus on a representative *pick-and-place* task, where the agent is instructed to pick up the target object and place it on the plate. In this task, observations consist of a 480×640 third-person image, joint-poses and instructions. Actions are defined in delta end-effector poses. This task provide three kinds of rewards:

- *outcome reward*: give a reward of +1 is the task succeed and 0 otherwise.
- *is grasp reward*: give a reward of +0.1 if the robot grasp the target object and 0 otherwise.
- *consecutive grasp reward*: give a reward of +0.1 if the robot grasp the target object for few steps and 0 otherwise.

B.1 Table Textures and Objects

We collect 21 different table textures and 25 different categories of objects, following the setup of RL4VLA[10]. The table textures are separated to 16 candidates for training environments and 5 candidates for evaluation environments. The objects are also splitted to the training set with 16 categories and the evaluation set with 9 categories. Only the table textures and objects belonging to the training set will be exposed to VLA models during SFT and RL training.

Table 3: RL fine-tuning and auxiliary-objective hyperparameters for OpenVLA and $\pi_{0.5}$. RL fine-tuning hyperparameters are shared by the PPO baseline and our method for each backbone; auxiliary-objective hyperparameters are used only by our method.

Parameter	OpenVLA	$\pi_{0.5}$
<i>RL fine-tuning</i>		
RL train steps	240	280
Global batch size	640	5120
Update epochs	1	5
Actor learning rate	1×10^{-4}	7.91×10^{-6}
Critic learning rate	3×10^{-3}	1.55×10^{-4}
Reward discount rate γ	0.99	0.99
GAE λ	0.95	0.95
PPO clip ratio ϵ	0.2	0.2
<i>Rollout collection</i>		
Interaction steps	80	80
Parallel environments	128	320
Rollout epochs	1	1
<i>Auxiliary objectives</i>		
Invariance coefficient α	1	4
Sensitivity coefficient β	0.2	4
Sensitivity clip c	0.8	0.08
<i>Action generation</i>		
Action prediction horizon H	1	8
Action replan horizon H'	1	5
Noise steps	–	4
Noise level σ (Flow-SDE)	–	0.5

B.2 Scene Lighting

The scene lighting is composed of a ambient light, a key light and two fill lights. As we want to test how the visual robustness learned from other kinds of variations transfer to OOD lighting conditions, the parameters of the scene lighting are fixed during SFT and RL training. Instead, we define 20 OOD lighting conditions by vary these parameters, which is held-out from training.

B.3 Object Position

For training, the positions of the objects are sampled from a square area centered at $[-0.16, 0]$ and length of the half-edge is 7.5cm. This square area is discretized to 6×6 grids and the initial positions are sampled from these grid points. Orientation is sampled from a set $\{0, \frac{1}{4}\pi, \frac{1}{2}\pi, \pi\}$. For evaluation, the square area is extended outward to half-edge ≈ 10.5 cm. The initialization position of the objects are sampled from the outer border.

B.4 Training and Evaluation Tasks

To systematically investigate the visual OOD robustness, we build multiple tasks as follows:

- *Training*: At the beginning of each episode, two objects are sampled from the training objects and one table texture is sampled from the training table textures. One of the sampled objects is the target object while another is the distractor. The appearance of the plate is fixed. Positions of the objects and the plate is sampled from the 6×6 grid in the small square area. The lighting condition is also fixed in the training task.
- *Unseen Table Texture*: The table texture is sampled from evaluation set. Other settings are the same as in *Training*.
- *Unseen Lighting*: The parameters of the lighting conditions are sampled the evaluation set with 20 different combinations. Other settings are the same as *Training*.

- *Unseen Pose* The position of the target object is sampled from outer border of the enlarged square area. Other settings are the same as *Training*.
- *Unseen Clutter* One object is sampled from the training set as the target object. N objects are sampled as distractors, where half of the objects are from training set and another half from evaluation set. We use "Distractor- N " to denote the task with N distractors. Other settings are the same as *Training*.

C Broader Impacts

Our work may have positive impact by improving the robustness and reliability of robot manipulation policies under visual shifts, which can reduce brittle failures in embodied AI systems such as assistive robots.

Potential negative impacts include unsafe deployment of visually robust policies in unvalidated real-world settings or misuse of improved robotic capabilities. We encourage proper and responsible use of our findings.